Article

Not peer-reviewed version

Dual Effect of Ag Doping and S Vacancy on H2 Detection for SnS2 Based Photo-Induced Gas Sensor at Room Temperature

Shaoling Wang , Xianju Shi , Ren-Jie Li , Na Fang , Haoran Ma , Ji-Chao Wang *

Posted Date: 28 April 2025

doi: 10.20944/preprints202504.2280.v1

Keywords: SnS2; gas sensor; Ag doping; light-activated; H2 detection

Article

Dual Effect of Ag Doping and S Vacancy on H_2 Detection for SnS_2 Based Photo-Induced Gas Sensor at Room Temperature

Shaoling Wang [1,2], Xianju Shi [1,2,*], Ren-Jie Li [3], Na Fang [1,2], Haoran Ma [4] and Ji-Chao Wang [4,*]

[1] School of Energy and Chemical Engineering, Puyang Vocational and Technical College, Puyang, 457000, China.
[2] Puyang Institute of Technology, Henan University, Puyang, 457000, China.
[3] XinXiang Hydrology and Water Resources Reporting Subcenter, Xinxiang, Henan, 453000, China.
[4] College of Chemistry and Chemical Engineering, Henan Institute of Science and Technology, Xinxiang, 453003, China.
* Correspondence: pyshixianju@163.com (X.S.); wangjichao@hist.edu.cn or wangjichao2016@163.com (J.-C.W.)

Abstract: Hydrogen (H_2) monitoring demonstrates significant practical importance for safety assurance in industrial production and daily life, driving the demand for gas sensing devices with enhanced performance and reduced power consumption. This study presented a room-temperature (RT) hydrogen sensing platform utilizing two-dimensional (2D) Ag-doped SnS_2 nanomaterials activated by light illumination. The Ag-SnS_2 nanosheets, synthesized through hydrothermal methods, exhibited exceptional H_2 detection capabilities under blue LED light activation. The synergistic interaction between silver dopants and photoactivation enabled remarkable gas sensitivity across a broad concentration range (5.0-2500 ppm), achieving rapid response/recovery times (4 s/18 s) at 2500 ppm under RT. Material characterization revealed that Ag doping induced S vacancy, enhancing oxygen adsorption, while simultaneously facilitating photo-induced hole transfer for surface hydrogen activation. The optimized sensor maintained good response stability after five-week ambient storage, demonstrating excellent operational durability. Experimental results further elucidated that Ag dopants enhancing hydrogen adsorption-activation while S vacancy improved surface oxygen affinity. This work provided fundamental insights into defect engineering strategies for developing optically modulated gas sensors, proposing a viable pathway for constructing energy-efficient environmental monitoring systems.

Keywords: SnS_2; gas sensor; Ag doping; light-activated; H_2 detection

1. Introduction

As a carbon-neutral energy carrier with high gravimetric energy density, hydrogen has emerged as a pivotal renewable energy source for applications ranging from chemical synthesis to fuel cell technologies and industrial combustion systems.[1] Yet, the widespread adoption of hydrogen energy necessitates urgent resolution of inherent safety concerns, particularly given its hazardous characteristics including a wide explosive concentration range (4.0-75.0 vol%), high diffusion coefficient (0.61 cm^2/s), and substantial combustion enthalpy (285.5 kJ/mol).[2–4] thus, it is of great significance to selectively detect trace hydrogen[5]. These intrinsic properties underscore the critical requirement for developing reliable detection systems capable of selective trace-level hydrogen monitoring (particularly <1000 ppm) in operational environments. Recently, Current hydrogen detection methodologies primarily employ analytical techniques such as gas chromatography (GC), semiconductor gas-sensor, and optical spectroscopy approaches[1,5] In contrast, semiconductor-based chemiresistive sensors have garnered significant research interest due to their inherent

 doi:10.20944/preprints202504.2280.v1

advantages of low-cost fabrication, scalable manufacturing processes, and balanced performance metrics in sensitivity-stability-selectivity.

SnS_2 materials, as a 2D layered transition metal disulfide, has been gradually regarded as promising gas-sensing materials, due to its large surface and great electrical character[6]. A series of SnS_2 based materials exhibited the good gas-sensitive property for NO_2, NH_3, Xylene, C_2H_5OH and H_2S molecules[7–11]. W. Gao et al. proven that Pd/SnS_2/SnO_2 sensor exhibited high response and response time to 500 ppm H_2 at 300 °C[4]. However, for activating the gas-detection ability of semiconductor, a high operating temperature range of 100-450 °C was typically required with an additional heater[12,13]. Facing with its high resistance and weak adsorption to H_2 molecule at room temperature(RT), the especial structure designing of SnS_2 surface and external non-thermal field condition played two crucial roles for solving the above issues[13,14]. Due to the excellent light absorption capacity of SnS_2, light irradiation could be an effective alternative to thermal driving to activate the adsorption behavior of gas molecules [14]. Under illumination, abundant electron-holes pairs could promote the electron transfer, further improving the gas-sensing properties. While UV illumination (λ < 400 nm) demonstrated effective photoactivation, its practical application is limited by photon-induced material degradation and potential health hazards. Recent advances in LED technology offer a safer alternative through visible light irradiation, combining sufficient photon energy for electron excitation with low power consumption[12]. Therefore, the synergistic combination of defect-engineered SnS_2 nanostructures and LED photoactivation to develop an energy-efficient H_2 sensor operating at RT.

Besides, the strategic introduction of sulfur vacancies (Vs) in SnS_2 lattices enables selective oxygen chemisorption through isovalent orbital interactions, capitalizing on the chalcogen-group electronic affinity that facilitates superoxide radical(O_2^-) formation at defect sites. Simultaneously, noble metal dopants with high work functions demonstrated superior hydrogen spillover effects, their d-orbital electron configurations enabling optimized hydrogen binding energies through charge-transfer interactions[15,16]. In the intrinsic 2D SnS_2 lattice, the Sn atom was sandwiched between two layers of S atoms maintained by van der Waals forces[17]. Doped Ag(I) impurity not only brought out the adsorbed-activate site for hydrogen, but also facilitated the formation of S vacancy due to charge and size difference between Ag(I) and Sn(IV) in SnS_2[17]. Thus, it would be of great interest to investigate the synergistic effect of S vacancy and Ag impurity on the sensing performance of Ag doped SnS_2 sensors.

In this regard, a series of Ag doped SnS_2 (Ag-SnS_2) sheet was synthesized and used as the sensing material in sensing H_2 with the help of LED light illumination. The photo-activated Ag-SnS_2 sheet showed a significantly enhanced H_2 sensing performance with wide serviceable range from 5.0 ppm to 2500 ppm at RT. Such excellent gas-sensitivity was attributed to the effect of Ag doping and light illumination. The influence of Ag doping on the surface structure was investigated by ESR and TEM. Additionally, through O_2 absorption measurement and in-situ X-ray photoelectron spectroscopy(XPS), the possible mechanism was proven.

2. Materials and Methods

The SnS_2 based sample was synthesized through the one-step solvothermal method. Initially, 2.5 mL Triton X-100, 5.0 mmol citric acid and 5.0 mmol $SnCl_4 \cdot 5H_2O$ were orderly dissolved in 30 mL of deionized water and then added into 0.15 mmol of $AgNO_3$ under stronger stirring conduction. The 5 mL of thioacetamide solution (2.0 mmol/mL) was slowly added into the above colloidal solution under stirring. After the ultrasonic processing for 30 min, the resulting mixture was transferred to the Teflon-lined autoclave and heated at 150 ℃ for 12 h. The Ag-SnS_2 composite was finally obtained by centrifugation and washed by water/ethanol (three times) with subsequent drying at 70 ℃. This sample was named as xAg-SnS_2, in which x was on behalf of the ideal ratio (mol/mol %) between Ag and Sn element. The pristine SnS_2 sample was prepared using the above similar method without addition of $AgNO_3$. The SnS_2 based gas sensors were formed and the synthesized process was detailed in supplementary materials S1. The gas-sensitive property was measured using

doi:10.20944/preprints202504.2280.v1

reconstructive W30-A gas-sensitive equipment (Figure S1)[18,19]. The structural characterization of the obtained SnS_2 samples were detailed in supplementary materials S2.

3. Results

As shown in Figure 1, five obvious peaks at 15.0°, 28.2°, 32.1°, 50.0° and 52.5° were corresponding to the characteristic peaks of (0 0 1), (1 0 0), (1 0 1), (1 1 0) and (1 1 1) plane of hexagonal-2T SnS_2 materials. With Ag addition, the intensity of one broad peak at about 22.0 ° gradually increased, while no new peak appeared. Based on the ICP-OES result (Table S1), Ag impurity was existed in the Ag-SnS_2 sample and its content increased with increasing Ag feedstock input. In the high resolution Sn 3d spectra (Figure 1b), two stronger peaks at the binding energies of 487.2 and 495.7 eV were associated with the Sn $3d_{5/2}$ and $3d_{3/2}$ of Sn(IV).[20,21] As displayed in Figure 1c, two peaks at 161.9 eV and 163.1 eV was corresponding to S $2p_{3/2}$ and $2p_{1/2}$, respectively (Figure 1c) [22,23]. In Figure 1d, two peaks at 368.0 and 374.1 eV were ascribed to $3d_{5/2}$ and $3d_{3/2}$ of Ag(I) [17,20]. The peak of both Sn and S shift negatively after Ag doping, indicating change of surroundings electronegativity around atom. In ESR spectra (Figure 1e), a clear sign of S vacancy (g=2.004) appeared in the sample of Ag doped SnS_2 and its intensity enhanced with increasing Ag input[17]. Combined with XRD result, the ordered arrangement of Sn-S was destroyed by doped Ag impurity, further forming the S vacancy. As shown in Figure S2, the sheet morphology appeared in SnS_2 and 3Ag-SnS_2 samples. In Figure 1f, the lattice fringes with spacing 0.278 and 0.182 nm were corresponding to the (1 0 1) and (1 1 0) crystal faces of hexagonal-2T SnS_2. Therefore, a series of Ag doped SnS_2 sheet with S vacancy were obtained through one-step hydrothermal process.

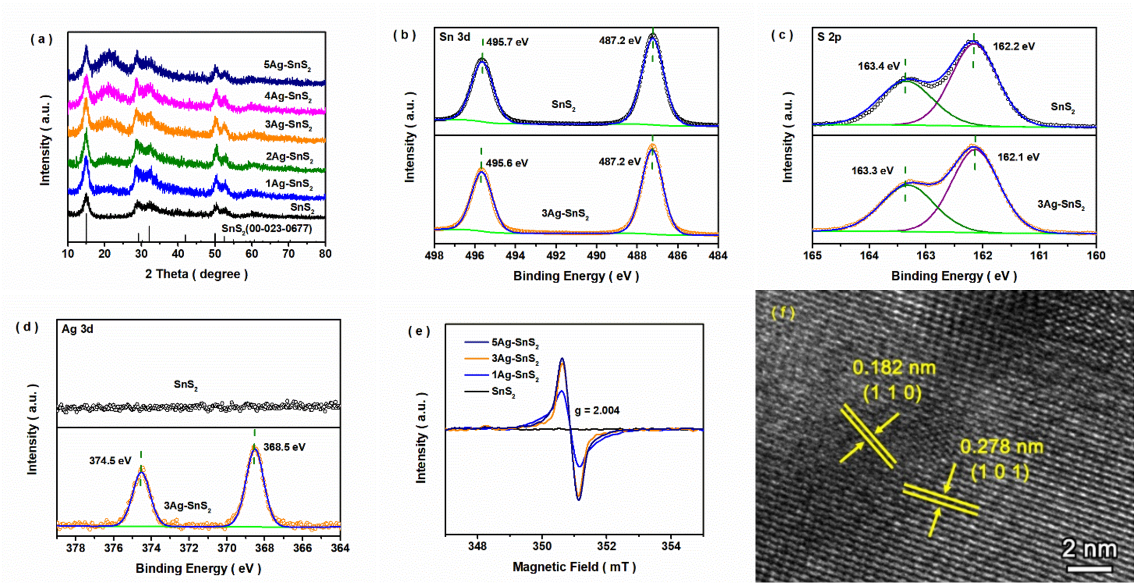

Figure 1. XRD, XPS, ESR and HR-TEM of SnS_2 and doped SnS_2 samples(**a**. XRD, **b**. XPS Sn 3d, **c**. XPS S 2p, **d**. XPS Ag 3d, **e**. ESR and **f**. HR-TEM of 3Ag-SnS_2 sample).

The gas-sensitive property for H_2 detection of SnS_2 based materials was investigated. In Figure 2a, all SnS_2 materials exhibited the sensitive property for H_2 gas at room temperature, and its response under illumination was apparently higher than that in dark. With increasing Ag addition, the response value of Ag-SnS_2 sensor was gradually promoted and 3Ag-SnS_2 sample showed the highest response value for H_2 detection. Beyond the optimal value, its sign exhibited a marked decline, which was caused by the excess defect in SnS_2 surface, further decreasing the concentration of active electron. For further exploring the liner between gas concentration and sensor sign, the results(Figure 2b) manifested that, although the fast response rate of 3Ag-SnS_2 photoinduced sensor appeared, its recovery time was gradually lengthened with increasing concentration of H_2 gas. Lucky, its response and recovery time in 2500 ppm H_2 condition still kept ~4 s and ~18 s, respectively. Besides, a linear

Preprints.org (www.preprints.org) | NOT PEER-REVIEWED | Posted: 28 April 2025 doi:10.20944/preprints202504.2280.v1

correlation (y=0.01498x+2.428, R^2 0.9923) could be determined between 5 ppm to 2500 ppm of H_2 concentration. In Figure 2c, facing with multiple different target gases, the 3Ag-SnS_2 sensor exhibited the good selectivity for H_2 gas. The cycling stably of gas sensor was not ignored. As shown in Figure 2d, the photoinduced gas sensor of 3Ag-SnS_2 exhibited the stable response value of H_2 detection at room temperature in 35 days. Compared with the previous SnS_2 or SnO_2 based gas sensor as summarized in Table S2, the 3Ag-SnS_2 photo-induced sensor exhibited the good sensitivity, selectivity and stability for H_2 detection with wide concentration range(5.0 to 2500 ppm) in operating temperature of room temperature[24–33].

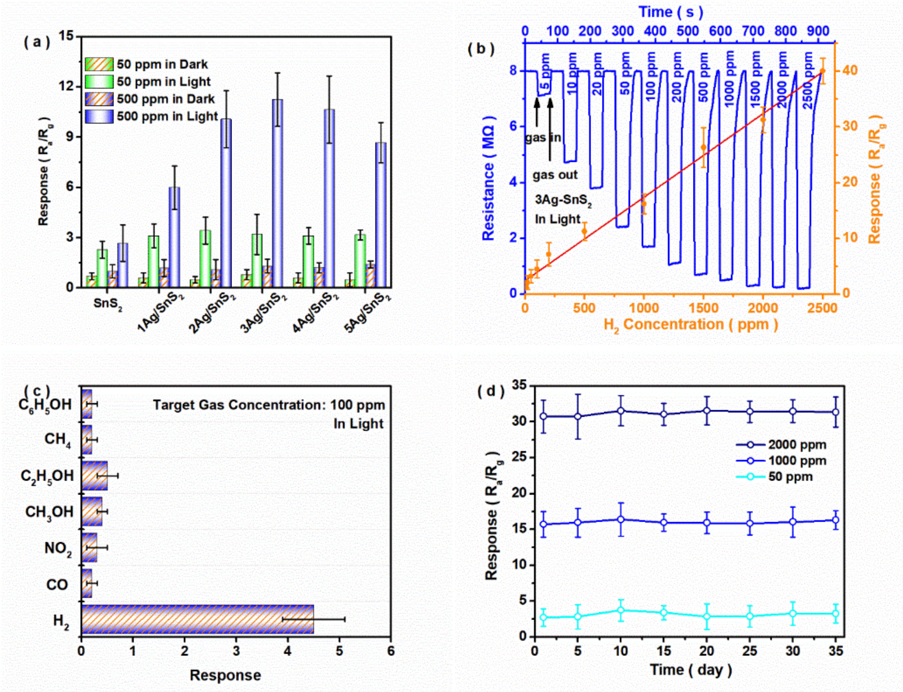

Figure 2. Performance of SnS_2 and Ag-SnS_2 based gas sensor(**a**. gas sensitivity for different samples; **b**. resistance and response of 3Ag-SnS_2 sensor for different H_2 concentration; **c**. gas selectivity of 3Ag-SnS_2 sensor for different sample; **d**. cycling stability of 3Ag-SnS_2 sensor in 5 weeks).

For exploring the reason about enhanced photo-induced gas sensitivity of Ag-SnS_2, the band structure and surface state of the obtained samples were further investigated. Firstly, the influence of Ag impurity on the band structure of SnS_2 was studied. In Figure 3a, the light-response ranges of 3Ag-SnS_2 sample showed wider than that of pristine SnS_2 and their Eg value were calculated and summarized in Table S3. Then the VB band position could be measured through VB-XPS measurement. With Ag doping, the VB value modest decreased in Figure 3b. Finally, the CB position could be calculated and the information about their band structure was summarized in Table S2. Additionally, the photoinduced current curve was showed in Figure S3. Although the photoinduced current density of Ag-SnS_2 exhibited all higher than that of SnS_2, excess Ag impurity never bring out more abundance photoinduced electrons. It was the possible reason that S vacancy was easily formed around doped Ag site due to the effect of charge balance, but superfluous vacancy made it a recombination center of photoinduced electron-holes, leading to the weak current density. This also explained that 3Ag-SnS_2 sample exhibited the better gas-sensitive property, compared with other.

 doi:10.20944/preprints202504.2280.v1

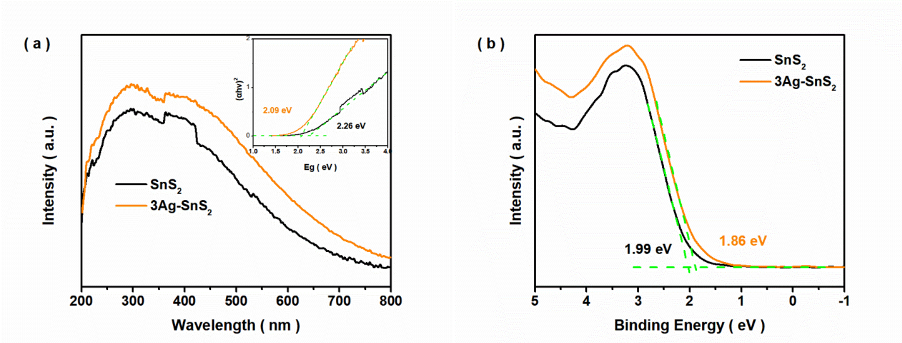

Figure 3. (**a**)DRS and (**b**)VB-XPS of the SnS_2 and 3Ag-SnS_2 samples.

In Figure 4a, all obtained samples showed the adsorptive property of O_2 gas at room temperature. It was notably that the existence of Ag impurity enhanced the O_2 adsorbing capacity of SnS_2 and its variation tendency agreed with the change of S vacancy(Figure 1e). In Figure 4b, the variation trend of H_2 adsorption property was similar to that of O_2 adsorbing. With increasing the density of Ag site on surface, the H_2 adsorbing capacity of SnS_2 was increased, which was due to the superior hydrogen-binding capability of high work function metal element. Additionally, the in situ-XPS result (Figure 4c) showed that the peak position of Ag impurity in light shifted toward high energy direction and it reversely moved after light off. It indicated that the electron in Ag site lose in light and this change of Ag atom in light/dark condition was reversible[34]. Hence, doped Ag site may play a role for surface transfer of photo-induced hole. Based on the above results, as shown in Figure 4c, the S vacancy around Ag site of surface could easily adsorbed the oxygen molecule. And then, metal Ag site could capture hydrogen molecule in air, which formed two neighboring adsorbed O_2/H_2 molecules. Simultaneously, under illumination, the photogenerated electron and hole transferred from SnS_2 to adsorbed O_2 and H_2 molecules, respectively. The superoxide radical(O_2^-) and hydrogen ion(H^+) were formed and reacted for each other, leading to electron consumption and the change resistance of SnS_2. The possible mechanism for H_2 detection of photoinduced gas sensor was showed in Figure 4d.

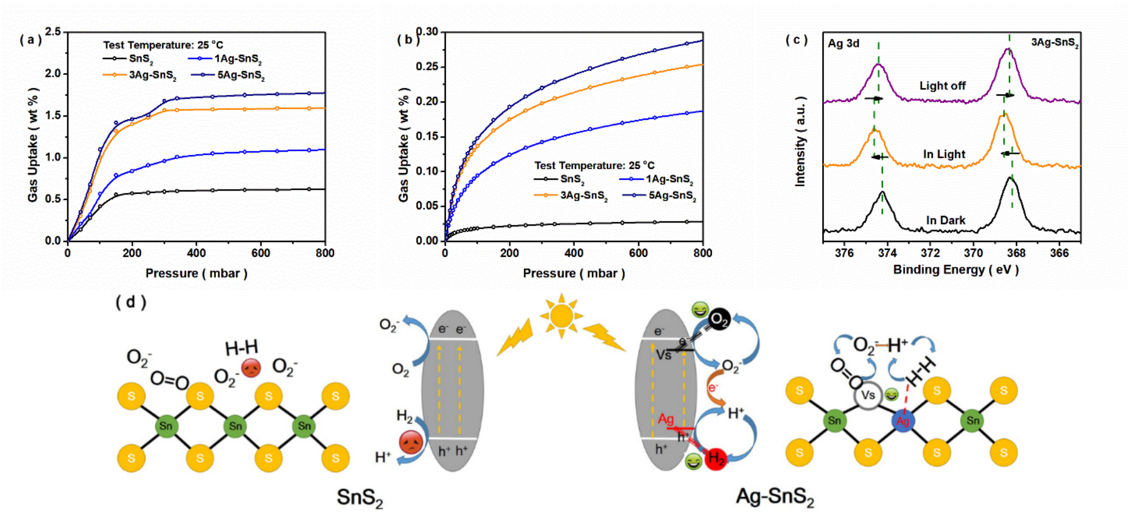

Figure 4. O_2 (**a**) and H_2 (**b**) absorption property for SnS_2 and Ag-SnS_2 samples, in situ XPS of Ag element in light/dark (**c**) and Schematic diagram of gas sensing mechanism (**d**).

4. Conclusions

In conclusion, a series of sheet-like Ag doped SnS_2 materials were prepared through the one-step hydrothermal method. The S vacancy was generated along with the Ag impurity doping, leading to enhanced O_2 adsorbed property. Compared to the pristine SnS_2, which was hard to sense H_2 at RT, the Ag-SnS_2 sample exhibited an excellent gas-sensitive property for H_2 detection with wide concentration range from 5.0 ppm to 2500 ppm under blue LED illumination. Facing with the high concentration condition of H_2 gas (2500 ppm), its response and recovery time still kept ~4 s and ~18 s, respectively. Moreover, the sensor maintained the gas response after five weeks of relaxation. The synergistic effect of S vacancy and Ag impurity on enhanced O_2/H_2 adsorbed property has been proven. The Ag impurity site played a key role for photo-induced hole transfer to active adsorbed hydrogen on SnS_2 surface under illumination. On account of remarkable gas sensing performances, the formation of Ag doped SnS_2 sheet contributed to enhance the potential and fueled the exploitation of next-generation high-performance gas sensing light modulated devices at RT.

Supplementary Materials: The following supporting information can be downloaded at the website of this paper posted on Preprints.org. S1. Gas sensing characterization. S2. Sample characterization. Figure S1. Gas sensing characterization. Figure S2. TEM images of SnS_2 and 3Ag-SnS_2 samples. Figure S3. Photoinduced current curve of SnS_2 and Ag-SnS_2 samples. Table S1. Element content of obtained SnS_2 sample by ICP-OES. Table S2. Gas-sensitive property of SnS_2 or SnO_2 based materials for H_2 detection in previous studies and researches. Table S3. Band structure of Ag-SnS_2 and SnS_2 materials. Figure S1. Schematic diagram of photoinduced-gas-sensor.

Author Contributions: Conceptualization, J.C.W. and X.S.; methodology, J.C.W.; software, R.J.L., N.F. and H.M.; validation, H.M.; formal analysis, R.J.L. and N.F.; investigation, H.M.; resources, R.J.L; data curation, S.W. and H.M.; writing—original draft preparation, S.W. and J.C.W.; writing—review and editing, J.C.W.; project administration, J.C.W.; funding acquisition, J.C.W. and X.S.. All authors have read and agreed to the published version of the manuscript.

Funding: This research was funded by Scientific and Technological Research Project of Henan Province(No. 252102230085 and 252102320178) and Training Program for Young Backbone Teachers in Higher Education Institutions in Henan Province (No. 2024GGJS101).

Conflicts of Interest: The authors declare no conflicts of interest.

References

1. Hjiri, M.; Dhahri, R.; Benmansour, N.; Neri, G. Laser irradiated gas sensors: A review. *Micro Nanostruct.* **2025,** 204, 208157. https://doi.org/10.1016/j.micrna.2025.208157
2. Liu, Y.; Chen, S.; Xiao, B.; Chu, J.; Wang, H.; Chen, Y.; Yao, T.; Yang, A.; Han, X.; Rong, M.; Wang, X. Ultra-large Sn_3O_4 nanosheets with Sn^{2+} defect for highly efficient hydrogen sensing. *Sens. Actuators, B* **2024,** *401*, 135025. https://doi.org/10.1016/j.snb.2023.135025
3. Yin, X.-T.; Wu, S.-S.; Dastan, D.; Nie, S.; Liu, Y.; Li, Z.-G.; Zhou, Y.-W.; Li, J.; Faik, A.; Shan, K.; Shi, Z.; Tarighat, M. A.; Ma, X.-G. Sensing selectivity of SnO_2-Mn_3O_4 nanocomposite sensors for the detection of H_2 and CO gases. *Surf. Interfaces* **2021,** *25*, 101190. https://doi.org/10.1016/j.surfin.2021.101190
4. Meng, X.; Bi, M.; Xiao, Q.; Gao, W. Ultrasensitive gas sensor based on Pd/SnS_2/SnO_2 nanocomposites for rapid detection of H_2. *Sens. Actuators, B* **2022,** *359*, 131612. https://doi.org/10.1016/j.snb.2022.131612
5. Zhu, M.; Zhang, H.; Zhang, S.; Yao, H.; Shi, X.; Xu, S. Chemoresistive gas sensors based on noble-metal-decorated metal oxide semiconductors for H_2 detection. *Materials*, **2025**, *18*, 451. https://doi.org/10.3390/ma18020451
6. Mishra, R. K.; Choi, H. J.; Ryu, J. W.; Choi, G. J.; Kumar, V.; Kumar, P.; Singh, J.; Kumar, S.; Gwag, J. S. Recent progress in gas sensing based on 2D SnS_2 and its heterostructure platforms: A review. *Sens. Actuators, A* **2024,** *365*, 114860. https://doi.org/10.1016/j.sna.2023.114860
7. Saggu, I. S.; Singh, S.; Chen, K.; Xuan, Z.; Swihart, M. T.; Sharma, S. Ultrasensitive room-temperature NO_2 detection using SnS_2/MWCNT composites and accelerated recovery kinetics by UV activation. *ACS Sensors* **2023,** *8*, 243-253. https://doi.org/10.1021/acssensors.2c02104
8. Lee, S. M.; Kim, Y. J.; Park, S. J.; Cheon, W. S.; Kim, J.; Nam, G. B.; Kim, Y.; Jang, H. W. In-situ growth of 2D MOFs as a molecular sieving layer on SnS_2 nanoflakes for realizing ultraselective H_2S detection. *Adv. Funct. Mater.* **2025,** *35*, 2417019. https://doi.org/10.1002/adfm.202417019

Preprints.org (www.preprints.org) | NOT PEER-REVIEWED | Posted: 28 April 2025 doi:10.20944/preprints202504.2280.v1

9. Qiu, P.; Qin, Y.; Wang, X. S-vacancies and Ag nanoparticles in SnS_2 nanoflakes for ethanol sensing: A combined experimental and theoretical investigation. *ACS Appl. Nano Mater.* **2022,** *5*, 10839-10847. https://doi.org/10.1021/acsanm.2c02153
10. Lu, Y.; Zhang, J.; Wang, W.; Fan, Y.; Liu, C.; Zhou, J.; Liu, D.; Ruan, S. Au-Pd modified SnS_2 nanosheets for conductometric detection of xylene gas. *Sens. Actuators, B* **2022,** *351*, 130907. https://doi.org/10.1016/j.snb.2021.130907
11. Maria, K. H.; Sakhuja, N.; Jha, R. K.; Bhat, N. Ultra-sonication assisted synthesis of 2D SnS_2 nanoflakes for room-temperature NO gas detection. *IEEE Sens. J.* **2021,** *21*, 10420-10427. https://doi.org/10.1109/JSEN.2021.3059087
12. Eom, T. H.; Cho, S. H.; Suh, J. M.; Kim, T.; Lee, T. H.; Jun, S. E.; Yang, J. W.; Lee, J.; Hong, S.-H.; Jang, H. W. Substantially improved room temperature NO_2 sensing in 2-dimensional SnS_2 nanoflowers enabled by visible light illumination. *J. Mater. Chem. A* **2021,** *9*, 11168-11178. https://doi.org/10.1039/D1TA00953B
13. Ramakrishnan, K.; Ajitha, B.; Ashok Kumar Reddy, Y. Review on metal sulfide-based nanostructures for photodetectors: From ultraviolet to infrared regions. *Sens. Actuators, A* **2023,** *349*, 114051. https://doi.org/10.1016/j.sna.2022.114051
14. Li, Q.; Wang, X.; Li, H.; Guo, X. Light-activated gas sensors. *Chin. Sci. Bull.* **2022,** *67*, 1837-1850. https://doi.org/10.1360/TB-2021-1075
15. Arain, S.; Usman, M.; Saeed, F.; Feng, S.; Rehman, W.; Liu, X.; Dai, H. Microemulsion-based synthesis of highly efficient Ag-doped fibrous SiO_2-TiO_2 photoanodes for photoelectrochemical water splitting. *Catalysts*, **2025**, *15*, 66. https://doi.org/10.3390/catal15010066
16. An, Q.; Li, J.; Peng, J.; Hu, L. DFT study of small gas molecules (C_2H_2, CH_4, CO and H_2) adsorbed on Au, Ag-doped ZnO monolayer. *Chem. Phys. Lett.* **2025,** *869*, 142043. https://doi.org/10.1016/j.cplett.2025.142043
17. Yang, H.; Du, Z.; Yang, Y.; Li, X.; Wu, Q.; Tang, J.; Wang, X.; Zeng, D. Ag intercalated SnS_2 with S vacancy and expanded interlayer for enhancing NO_2 sensing. *Sens. Actuators, B* **2023,** *393*, 134140. https://doi.org/10.1016/j.snb.2023.134140
18. Wang, J.-C.; Ma, H.; Shi, W.; Li, W.; Zhang, Z.; Hou, Y.; Zhang, W.; Chen, J. Designed synthesized step-scheme heterojunction of Bi_2WO_6 nanosheet supported on $CuBi_2O_4$ nanorod with remarkable photo-assisted gas sensing for N-butyl alcohol. *J. Environ. Chem. Eng.* **2024,** *12*, 112698. https://doi.org/10.1016/j.jece.2024.112698
19. Wang, J.-C.; Shi, W.; Sun, X.-Q.; Wu, F.-Y.; Li, Y.; Hou, Y. Enhanced photo-assisted acetone gas sensor and efficient photocatalytic degradation ssing Fe-doped hexagonal and monoclinic WO_3 phase−junction. *Nanomaterials*, **2020**, *10*, 398. https://doi.org/10.3390/nano10020398
20. Tian, W.; Han, J.; Wan, L.; Li, N.; Chen, D.; Xu, Q.; Li, H.; Lu, J. Enhanced piezocatalytic activity in ion-doped SnS_2 via lattice distortion engineering for BPA degradation and hydrogen production. *Nano Energy* **2023,** *107*, 108165. https://doi.org/10.1016/j.nanoen.2023.108165
21. Lv, Y.-R.; Wang, Z.-L.; Yang, Y.-X.; Luo, Y.; Yang, S.-Y.; Xu, Y.-H. Tin bisulfide nanoplates anchored onto flower-like bismuth tungstate nanosheets for enhancement in the photocatalytic degradation of organic pollutant. *J. Hazard. Mater.* **2022,** *432*, 128665. https://doi.org/10.1016/j.jhazmat.2022.128665
22. Lei, Z.; Wang, W.; Sun, T.; Liu, E.; Gao, T. Efficient photocatalytic H_2 evolution over SnS_2/twinned $Mn_{0.5}Cd_{0.5}S$ hetero-homojunction with double S-scheme charge transfer routes. *J. Mater. Sci. Technol.* **2025,** *216*, 81-92. https://doi.org/10.1016/j.jmst.2024.07.034
23. Mamo, T. T.; Qorbani, M.; Hailemariam, A. G.; Putikam, R.; Chu, C.-M.; Ko, T.-R.; Sabbah, A.; Huang, C.-Y.; Kholimatussadiah, S.; Billo, T.; Hussien, M. K.; Chang, S.-Y.; Lin, M.-C.; Woon, W.-Y.; Wu, H.-L.; Wong, K.-T.; Chen, L.-C.; Chen, K.-H. Enhanced CO_2 photoreduction to CH_4 via *COOH and *CHO intermediates stabilization by synergistic effect of implanted P and S vacancy in thin-film SnS_2. *Nano Energy* **2024,** *128*, 109863. https://doi.org/10.1016/j.nanoen.2024.109863
24. Qin, Y.; Zhang, Y.; Qiu, P.; Lei, S. SnO_2-Co_3O_4 nanocomposite sensor: Achieving ultra-selective hydrogen detection in mixed gas environments. *Sens. Actuators, B* **2025,** *422*, 136521. https://doi.org/10.1016/j.snb.2024.136521

 doi:10.20944/preprints202504.2280.v1

25. Li, A.; Zhao, S.; Bai, J.; Xiao, H.; Gao, S.; Shen, Y.; Yuan, Z.; Meng, F. The role of AuSn alloys in optimizing SnO_2 nanospheres for chemoresistive hydrogen sensing. *Sens. Actuators, B* **2025,** *427*, 137214. https://doi.org/10.1016/j.snb.2024.137214
26. Liu, Y.; Chen, S.; Xiao, B.; Chu, J.; Wang, H.; Chen, Y.; Yao, T.; Yang, A.; Han, X.; Rong, M.; Wang, X. Ultra-large Sn_3O_4 nanosheets with Sn^{2+} defect for highly efficient hydrogen sensing. *Sens. Actuators, B* **2024,** *401*, 135025. https://doi.org/10.1016/j.snb.2023.135025
27. Liu, W.; Zou, J.; Li, S.; Li, J.; Li, F.; Zhan, Z.; Zhang, Y. Pd/In_2O_3-based bilayer H_2 sensor with high resistance to silicone toxicity and ultra-fast response. *Int. J. Hydrogen Energy* **2023,** *48*, 5743-5753. https://doi.org/10.1016/j.ijhydene.2022.11.043
28. Meng, X.; Bi, M.; Xiao, Q.; Gao, W. Ultrasensitive gas sensor based on Pd/SnS_2/SnO_2 nanocomposites for rapid detection of H_2. *Sens. Actuators, B* **2022,** *359*, 131612. https://doi.org/10.1016/j.snb.2022.131612
29. Lu, S.; Zhang, Y.; Liu, J.; Li, H.-Y.; Hu, Z.; Luo, X.; Gao, N.; Zhang, B.; Jiang, J.; Zhong, A.; Luo, J.; Liu, H. Sensitive H_2 gas sensors based on SnO_2 nanowires. *Sens. Actuators, B* **2021,** *345*, 130334. https://doi.org/10.1016/j.snb.2021.130334
30. Tang, C.; Jin, W.; Xiao, X.; Qi, X.; Ma, Y.; Ma, L. Graphene-based chemiresistive hydrogen sensor for room temperature operation. *Sens. Actuators, B* **2025,** *424*, 136889. https://doi.org/10.1016/j.snb.2024.136889
31. Kumar, G.; Li, X.; Du, Y.; Geng, Y.; Hong, X. UV-light enhanced high sensitive hydrogen (H_2) sensor based on spherical Au nanoparticles on ZnO nano-structured thin films. *J. Alloys Compd.* **2019,** *798*, 467-477. https://doi.org/10.1016/j.jallcom.2019.05.227
32. Wang, F.; Hu, K.; Liu, H.; Zhao, Q.; Wang, K.; Zhang, Y. Low temperature and fast response hydrogen gas sensor with Pd coated SnO_2 nanofiber rods. *Int. J. Hydrogen Energy* **2020,** *45*, 7234-7242. https://doi.org/10.1016/j.ijhydene.2019.12.152
33. Pandey, G.; Lawaniya, S. D.; Kumar, S.; Dwivedi, P. K.; Awasthi, K. A highly selective, efficient hydrogen gas sensor based on bimetallic (Pd–Au) alloy nanoparticle (NP)-decorated SnO_2 nanorods. *J. Mater. Chem. A* **2023,** *11*, 26687-26697. https://doi.org/10.1039/D3TA05878F
34. Wang, Z.; Cheng, B.; Zhang, L.; Yu, J.; Tan, H. BiOBr/NiO S-scheme heterojunction photocatalyst for CO_2 photoreduction. *Sol. RRL* **2022,** *6*, 2100587. https://doi.org/10.1002/solr.202100587